How ions distribute in a drying porous medium - a simple model

How ions distribute in a drying porous medium: A simple model

H. P. Huinink,[a] L. Pel, and M. A. J. Michels
Department of Applied Physics, Technische Universiteit Eindhoven, P.O. Box 513, 5600 MB Eindhoven, The Netherlands

(Received 16 January 2001; accepted 26 December 2001; published 5 March 2002)

Salt crystallization at surfaces is an important problem for buildings and monuments. We do not consider the formation of salt crystals as such, but focus on transport properties of ions in a drying porous medium. We deal with the first phase of the drying process, where the water is still uniformly distributed throughout the medium. An approximate model is presented, which accounts for both convection and diffusion. It is shown that the key parameter is the Peclet number at the evaporating surface, $\mathrm{Pe} \equiv hL/\varepsilon D$, where h, L, ε, and D are the drying rate, sample size, porosity, and diffusion constant, respectively. When $\mathrm{Pe} \ll 1$ (diffusion dominates over convection) the ions remain uniformly distributed throughout the system. Strong accumulation at the evaporating surface occurs for $\mathrm{Pe} \gg 1$ (convection dominates over diffusion). Crossover behavior is found for $\mathrm{Pe} \approx 1$. Therefore, it is likely that the first crystals will be formed both in the bulk and at the interfaces of the material when $\mathrm{Pe} \ll 1$. For high values of Pe the density peak at the evaporating surface will reach the saturation concentration long before it is reached in the bulk of the material. As a consequence, the salt starts to crystallize at the interfaces. © *2002 American Institute of Physics.*
[DOI: 10.1063/1.1451081]

I. INTRODUCTION

An important issue in building physics is the crystallization of salts in porous materials.[1,2] Many monuments and ancient buildings suffer from it, because crystal growth inside the stones causes crack formation. In the spring large spots of salt crystals blot many new buildings made of fired-clay bricks. Initially, the stones contain water with ions dissolved in it. Either by airflow around the building or by an increase of the temperature the stones start to dry. During this drying process the ion concentration increases until the saturation concentration is reached and the salt crystallizes.

An interesting aspect of these processes is that in many cases crystal growth preferably takes place at or in a region near the surface of the porous material. This behavior is poorly understood because it is not easy to measure ion concentration inside a porous material. Until now, most of the experimental work on this topic was done with destructive techniques, which have serious drawbacks. They are very time consuming; experiments cannot be repeated with the same sample, which causes considerable scatter in the data. Moreover, the resolution is limited by the mechanical treatment of the samples. As a consequence, systematic experiments are scarce and little is known of the origins of this tendency of crystals to form near the surface. Recently, it has been shown that NMR is a powerful technique for measuring the combined transport of Na^+ and water.[3] Due to the nondestructive nature of the technique and its ability to measure ^{23}Na and ^{1}H signals simultaneously, it is a powerful technique for studying the combined drying and crystallization process. In this paper, we do not want to investigate the crystallization process as such. We want to answer the following questions: How do ions distribute inside a porous medium during drying before any crystallization occurs? What does this tell us about the localization of crystals in the material? We do not take into account crystallization explicitly. The spots where the first crystals start to grow are the spots where the saturation concentration is reached first. However, we want to keep the model as simple as possible to be sure that we really understand the transport phenomena before we investigate a model, including crystallization.

To answer these questions, we derive a simple model based on the convection-diffusion equation. We limit ourselves to the so-called first drying stage.[4,5] This stage of the drying process covers an important part of the drying process, because approximately 60% of all water evaporates in this regime. This stage has the nice feature that the water remains uniformly distributed throughout the medium, which makes the analysis of the equations simpler. Both analytical and numerical outcomes will be discussed. The model was developed to gain more insight into the important parameters of the process and may serve as a guide for NMR experiments and computer simulations that we want to do in the near future.

The motion of ions in a drying porous medium is closely related to the transport behavior of ions during a phenomenon called ''wick action.'' [6,7] In both cases, the salt transport can be described in terms of the convection–diffusion equation and is driven by convective fluxes induced by evaporation. The fact that ion transport during drying requires a model of its own is caused by two important differences between wick action and drying. First, during wick action the water saturation is constant, the porous material is connected with a liquid reservoir, and the liquid velocity does not vary

[a]Author to whom correspondence should be addressed. Electronic mail: h.p.huinink@tue.nl

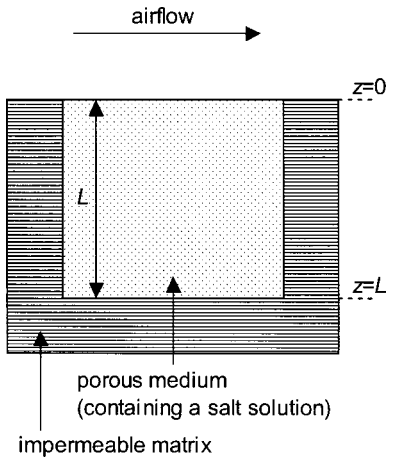

FIG. 1. Schematic picture of the drying system.

in position and time, given that the evaporating rate is constant. During a drying process the water saturation decreases. We will show that due to the variations in the water saturation the liquid velocity becomes time and position dependent. The second difference between wick action and drying is that the total amount of ions is conserved in the latter process. As already mentioned, wick action occurs in a porous material connected with a liquid reservoir containing ions (salt solution), i.e., the sea. First, in Sec. II we investigate the convection–diffusion model describing the process of interest. We subsequently discuss the partial differential equation and its boundary conditions, the analogy with the behavior of a Brownian particle in a potential well, and the length and time scales of the problem. Section III is dedicated to numerical solutions of this model. Analytic solutions are investigated in Sec. IV. In Sec. V we will draw conclusions and discuss the implications for salt crystallization.

II. CONVECTION–DIFFUSION MODEL

A. Starting point

The system we consider is a homogeneous porous cylinder of length L (m) with porosity ε (m^3/m^3) initially saturated with a salt solution. The liquid water saturation θ (m^3/m^3) is defined as the volume of water present in a given volume of the system. The maximal value of θ equals ε. A conceptual model of the system is drawn in Fig. 1. At the top ($z=0$) the solution is in contact with air, and water vapor can escape from the medium here. All other boundaries are sealed. Due to the airflow above the top surface, the density of the water vapor outside the porous material is kept at a constant value that is smaller than the equilibrium vapor density of the electrolyte. As a consequence, the system loses water, and the porous slab slowly dries. We assume that the evaporation process is isothermal, which is true in the case of slow drying.[8] At least two stages can be distinguished in the drying process.[4,5] In the first stage, the mass transfer at the top surface ($z=0$) is the limiting step in the water transport. As a consequence, only a small gradient in the water saturation θ (m^3/m^3) develops and the water saturation can be assumed to be equal to its volume-averaged value, $\theta \approx \langle \theta \rangle$. At a certain saturation level, the evaporation rate drops dramatically and a front develops and moves into the material. As mentioned before, we will only consider the first stage of the drying, where the water stays uniformly distributed throughout the sample.

In our system there is liquid flow in the direction of the evaporating surface. Therefore, an ion not only moves due to Brownian motion (diffusion), but it is dragged by the liquid too (convection). Convection drives the ions toward the evaporating surface, where they accumulate. Brownian motion tends to spread the ions uniformly over space. Obviously, a good description of the interplay of convection and diffusion is important. The convection–diffusion equation for unsaturated media serves[9] as a starting point for the description of the system. We assume that the amount of ions that adsorb on the pore walls is neglible. This assumption holds for materials with reasonably wide pores (>1 μm) like clay bricks and sand stones. By assuming electroneutrality, we do not have to treat the transport of both ions separately,[10] so we have

$$\frac{\partial c\theta}{\partial t} = \frac{\partial}{\partial z}\left(\theta D \frac{\partial c}{\partial z} - c\theta U \right), \tag{1}$$

where c (m^{-3}) is the number density of the electrolyte in the liquid phase and U (m/s) is the average velocity of the liquid at position z and time t. In Eq. (1) $D \equiv D_w/T$ (m^2/s), where D_w (m^2/s) and T are the diffusion constant of the electrolyte in the liquid phase and the electrical tortuosity factor, respectively,[11] which is a measure for the tortuosity of the liquid water network inside the porous medium. The first term on the rhs of Eq. (1) accounts for diffusion and the second term for convection. By using (1) we assume that hydrodynamic dispersion is negligible. This assumption holds when $|UR/D| \ll 1$ (R is the characteristic pore size of the medium),[12] which generally is the case for the experiments we have in mind ($D \approx 10^{-9}$ $m^2/s, R \approx 10^{-6}$ m, $U \approx 10^{-8}$ m/s). A second assumption in Eq. (1) is that the water network has no fractal properties on a length scale L. Therefore, this equation cannot account for anomalous diffusion and will break down for low values of θ close to the percolation threshold, where the liquid water network breaks up into isolated clusters. We expect this to occur when θ reaches the order of $0.1–0.3\varepsilon$.[13] However, this assumption does not narrow the application range significantly, because we have already limited ourselves to the first drying stage ($\theta > 0.4\varepsilon$). Finally, we have to remark that in the remainder of the paper we will consider T to be constant. Generally, T increases with decreasing θ. Although this certainly influences the details of the dynamics of the process, the qualitative picture does not change.

Using the fact that θ does not vary significant with z, and that $\rho = c\theta$ (the number density of the electrolyte), we can write Eq. (1) as follows:

$$\frac{\partial \rho}{\partial t} = D\frac{\partial^2 \rho}{\partial z^2} - \frac{\partial \rho U}{\partial z},$$
$$D\frac{\partial \rho}{\partial z} - \rho U = 0, \quad \text{at } z = 0, L. \tag{2}$$

In Sec. II B we will derive an expression for U. It is well known that Eq. (2) is a specific form of the Fokker–Planck (FP) equation.[14] This enables us to interpret U in terms of an external potential $V(U \equiv -D\partial V/\partial z)$. We will refer to V as the viscous potential.

B. Liquid velocity and viscous potential

The liquid velocity U and the viscous potential V depend on the details of the drying process. Even when the water is uniformly distributed throughout the medium, the liquid velocity U becomes dependent on t and z. The quantities θ and U are related to each other via the law of mass conservation:

$$\frac{\partial \theta}{\partial t} + \frac{\partial}{\partial z}(U\theta) = 0. \tag{3}$$

In Sec. II A we have already mentioned that we focus on the drying regime where the liquid is uniformly distributed throughout the porous slab. To solve Eq. (3) we assume that the evaporation rate h ($\mathrm{m/s} = \mathrm{m^3/m^2\,s}$) is time independent. This can be justified as follows. Under constant external conditions, a period with a constant drying rate is generally observed.[5] Recently, it has been shown with pore network simulations[15] that this constant-rate period is closely associated with the first drying regime, where variations in θ with z are negligible. The vapor pressure just below the top surface stays close to the equilibrium vapor pressure of water. We obtain the following expressions for U and θ, by solving Eq. (3):

$$U = \frac{h}{\theta L}(z - L), \tag{4}$$

$$\theta = \varepsilon - \frac{ht}{L}. \tag{5}$$

We use the boundary condition that there is no water transport possible through the bottom face, $U = 0$ at $z = L$, and the fact that the initial water saturation equals the porosity ε. Note that we did not use an explicit expression for the permeability to calculate U. This is a consequence of the fact that we use known saturation profiles (the uniform distribution of water) in combination with the law of mass conservation in the derivation.

The viscous potential is obtained by integrating (4):

$$V = \begin{cases} \infty, & z < 0 \\ -\dfrac{hL}{2D\theta}\left(\dfrac{z}{L} - 1\right)^2, & 0 \leqslant z \leqslant L, \\ \infty & z > L, \end{cases} \tag{6}$$

where we have set the integration constant to zero and used $U = 0$ outside the slab. The shape of this potential already contains a great deal of information about the characteristics of the transport process. From Eq. (6) it follows that our problem is equivalent to the problem of a Brownian particle in a potential well with a time-dependent shape. The infinitely high potential at the boundaries of the system guarantees the conservation of mass and gives rise to the reflecting-boundary conditions (2).

C. Length and time scales

In the preceding section we investigated the relation between drying and the liquid velocity. This enables us to identify the important length and time scales of our problem. From (6) we can conclude that two length scales characterize our problem: (a) the sample size L and (b) the one related with the transport processes, ξ,

$$\xi = \frac{D\varepsilon}{h}. \tag{7}$$

Below the length scale ξ, diffusion becomes dominant over convection (at $t = 0$). The depth of the viscous potential V increases when L/ξ increases (convection becomes more important on the length scale of the sample). Therefore, L/ξ is the key parameter for the process of salt accumulation at the surface ($z = 0$). Note that ξ is closely related to the Peclet number at $z = 0$ and $t = 0$ via Eq. (4),

$$\mathrm{Pe} \equiv \left|\frac{\tilde{U}L}{D}\right| = \frac{hL}{D\varepsilon} = \frac{L}{\xi}, \tag{8}$$

where $\tilde{U}$ is the liquid velocity at the evaporating surface at time $t = 0$. Both ξ and Pe are of great practical value, because h, ε, D, and L can be easily obtained from experiments or literature data. From now on we will refer to Pe at $z = 0$ and $t = 0$, defined in (8), as *the* Peclet number of the system. By using the typical values $h \approx 10^{-8}$ m/s, $L \approx 0.05$ m, $D \approx 10^{-9}$ m^2/s, and $\varepsilon \approx 0.1$, we estimate $\xi \approx 0.01$ m and $\mathrm{Pe} \approx 5$.

Just as we can characterize our problem by two length scales, we can also do this with two time scales: (a) the diffusion time $\tau_D \equiv L^2/D$ and (b) the drying time $\tau_\theta \equiv \varepsilon L/h$. With these definitions we can rewrite (8) as follows:

$$\mathrm{Pe} \equiv \tau_D/\tau_\theta. \tag{9}$$

The importance of Pe becomes clear when Eq. (2) is combined with (4), and a dimensionless time $s \equiv t/\tau_D$ and height $y \equiv z/L$ are introduced,

$$\frac{\partial \rho}{\partial s} = \frac{\partial^2 \rho}{\partial y^2} - \frac{\mathrm{Pe}}{1 - s\,\mathrm{Pe}}\frac{\partial}{\partial y}[\rho(y-1)], \tag{10}$$

$$\frac{\partial \rho}{\partial y} - \frac{\mathrm{Pe}}{1 - s\,\mathrm{Pe}}\rho(y-1), \quad \text{at } y = 0,1. \tag{11}$$

From Eq. (10), we can conclude that the transport behavior of the electrolyte is determined by one single parameter, Pe.

III. NUMERICAL CALCULATIONS

A. Procedure

Having obtained an expression for U and V, we can solve the convection–diffusion equation (2) to obtain the ion density distributions. However, the evaluation of this equa-

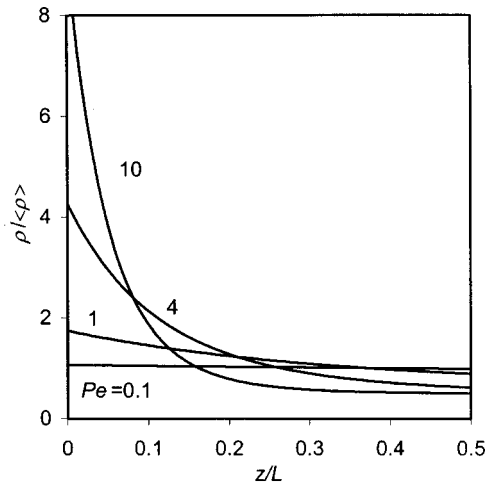

FIG. 2. Ion density profiles for different Peclet (Pe) numbers at $t=\tau_\theta/2$.

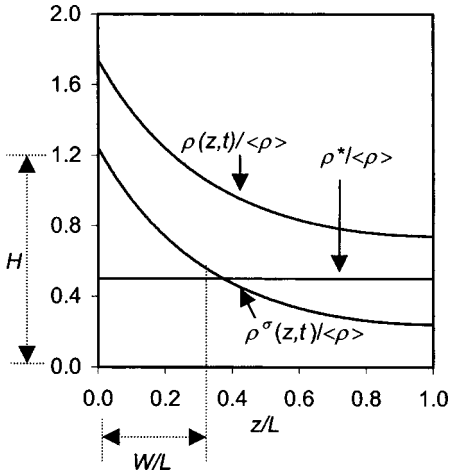

FIG. 3. An example (Pe$=1$,$t=\tau_\theta/2$) of the density profiles and excess density profiles, $\rho(z,t)$ and $\rho^\sigma(z,t)\equiv\rho(z,t)-\rho^*$, to illustrate the parameters W (peak width), H (peak height) and $\rho^\sigma(L,t)$ that are used to characterize such profiles.

tion is complicated by nonlinearity introduced by the time dependence of θ. Before we try to find analytical solutions, we evaluate this equation numerically with the help of a simple first-order one-sided finite difference (FD) scheme. This has the following advantages: we do not have to make additional assumptions, a complete overview of the behavior of Eq. (10) is obtained, and the outcomes can guide us in our search for analytical solutions.

Changes in the density at a node n can be calculated with the mass fluxes J with

$$\rho_n^{i+1}=\rho_n^i+\frac{\Delta t}{b}(J_{n,n+1}^i-J_{n-1,n}^i) \tag{12}$$

and

$$J_{n,n+1}^i=-\frac{D}{b}(\rho_n^i-\rho_{n+1}^i)+U_{n+1}^i\rho_{n+1}^i, \tag{13}$$

where b is the distance between two grid points, ρ_n^i and ρ_n^{i+1} are the densities at grid point n at times i and $i+1$, Δt is the time step, and U_{n+1}^i is the liquid velocity at $n+1$ and i. Note that (13) only holds when the liquid flow is in the $-z$ direction. At the boundaries nodes $n=0$ and $n=m$ $J_{-1,0}^i=J_{m,m+1}^i=0$. Equations (12) and (13) change into Eq. (2) for $b\to 0$ and $\Delta t\to 0$.

To prevent "numerical" diffusion, b has to be chosen such that $|Ub/D|\sim \mathrm{Pe}\, b/L\ll 1$. In the calculations we use $b/L=5\times10^{-3}$, which is suitable for Pe$=[0,10]$. Finally, we want to remark that this FD scheme is stable as long as $D\Delta t/b^2<0.5$. We have solved (2) for different values of Pe for $t=[0,\tau_\theta/2]$.

B. Density profiles

In Sec. II C we conclude that the key parameter to our problem is the Peclet number, $\mathrm{Pe}=hL/D\varepsilon$. In Fig. 2, we have plotted the ion distributions, $\rho/\langle\rho\rangle$, for various values of Pe at $t=\tau_\theta/2$. Here $\langle\rho\rangle$ is the volume-averaged density of the system. Clearly, the ion distribution is extremely sensitive to Pe. For Pe$\ll 1$($\xi\gg L$) the ions remain uniformly distributed throughout the medium due to the dominance of diffusive transport. Around Pe$=1$ ($\xi\approx L$) the crossover from diffusive to convective transport takes place, resulting in a significant accumulation of ions in a region near the evaporating surface. For Pe$\gg 1$ ($\xi\ll L$) convection dominates and the ions are strongly "attracted" by the top surface. For Pe$\to\infty$ the model gives the following density profile:

$$\rho(z,t)=\langle\rho\rangle\left(1+\frac{ht}{L\varepsilon}[L\,\delta(z)-1]\right), \tag{14}$$

where $\delta(z)$ is the Dirac-delta function. In reality, the density does not grow to infinity. At a certain moment the saturation concentration is reached and the ions crystallize. Although complete density profiles, shown in Fig. 2, contain much information, they are not very easy to use in a more systematic study. From now on we describe the ion distribution with an excess density profile, $\rho^\sigma(z,t)\equiv\rho(z,t)-\rho^*$ with $\rho^*=\langle\rho\rangle(1-ht/L\varepsilon)$ [see Eq. (14)]. Although we could have chosen a different definition for ρ^σ, this specific definition will prove to be very useful for describing the initial behavior of the ion density profiles in Secs. III C and IV. We will characterize ρ^σ with two different parameters: (a) $H(t)\equiv\rho^\sigma(0,t)/\langle\rho\rangle$, which is the height of the density peak at $z=0$; and (b) $W(t)$, defined as

$$W(t)\equiv\int_0^L\rho^\sigma z\,dz\Big/\int_0^L\rho^\sigma dz, \tag{15}$$

which is a measure for the width of the density peak. To clarify these definitions, we have plotted ρ and ρ^σ for Pe$=1$ at $t=\tau_\theta/2$ in Fig. 3. In the following sections we use H and W to subsequently study the initial growth of the height and width of the density distribution (Sec. III C) and the late-stage behavior of the peak (Sec. III D).

C. Initial growth of the density peak

More information about the shape of the density peak near $z=0$ can be obtained by calculating the peak width W and height H, plotted in Figs. 4(a) and 4(b), respectively. By

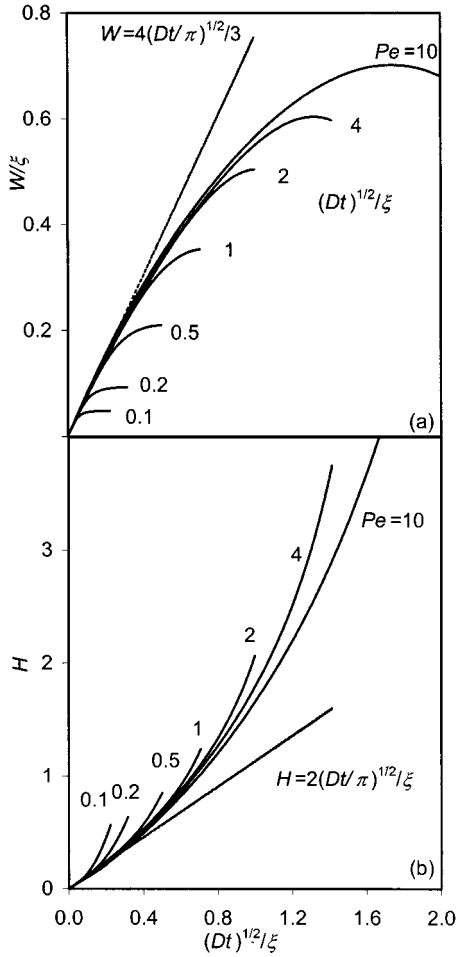

FIG. 4. The peak width W (a) and height H (b) as a function of time for different values Pe. The straight lines represent analytical results, derived in Sec. IV.

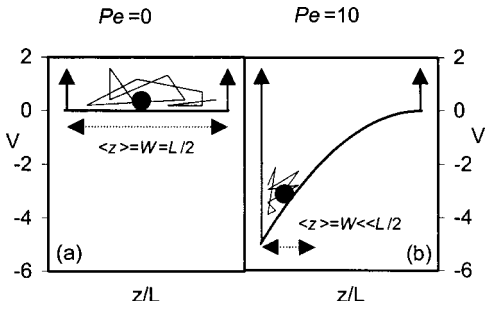

FIG. 5. Schematic picture of the behavior of a Brownian particle in a viscous potential V: (a) low Pe number (Pe$=0$) and (b) high Pe number (Pe $=10$). At Pe$=0$ the ions spread uniformly over space and the average distance of an ion to the evaporating surface equals $W=L/2$. At Pe$=10$ the ions are confined by the viscous potential in a region close to $z=0$ ($W \ll L/2$).

plotting these properties against $\sqrt{t}$, diffusive behavior can easily be discovered. These graphs contain two interesting features: (a) for small t both W and H scale with $\sqrt{t}$, and (b) when t increases W no longer scales with $\sqrt{t}$ and goes to a maximum value (this is discussed in the next section, Sec. III D).

To explain the "short-time" behavior of $\rho^{\sigma}(z,t)$ it is important to focus on the difference between W and H. Whereas H is seen to vary with h, ε, and D (H is a function of ξ), W is independent of h and ε. The fact that W does not depend on h and ε, being parameters that characterize the liquid flow, but does grow with $\sqrt{t}$, suggests that the broadening of the peak is a purely diffusive process. For small t the viscous-potential difference felt by diffusing ions is small and the diffusion process is not biased into a certain direction.

The ξ dependence and $\sqrt{t}$ scaling of H result from the behavior of the total excess amount of ions, Γ^{σ}, calculated as follows:

$$\Gamma^{\sigma} \equiv \int \rho^{\sigma}(z,t)\,dz = \langle \rho \rangle h t/\varepsilon. \tag{16}$$

When we assume that HW is proportional to Γ^{σ} (the peak area of ρ^{σ}), it follows from the combination of (16) and $W \propto \sqrt{Dt}$ that $H \propto \sqrt{Dt}/\xi$. This is in agreement with Fig. 4(b).

The behavior of the density peak (as described by W and H) indicates that it should be possible to derive an analytical expression for $\rho^{\sigma}(z,t)$ for small t. It follows from the scaling behavior of W and H that this expression should have the following mathematical form:

$$\rho^{\sigma}(z,t) = \langle \rho \rangle \frac{\sqrt{Dt}}{\xi} g\left(\frac{z}{\sqrt{Dt}}\right), \tag{17}$$

where the function g does not contain any other physical parameter than $z/\sqrt{Dt}$. In Sec. IV, the exact form of g and the expressions for W and H (as shown in Fig. 4) is derived. Equation (17) makes clear that initially the shape of the density peak formed at the evaporating surface does not depend on the sample size.

D. Late-stage behavior of the density peak

In the previous section we studied the initial growth of both the width and the height of the density peak. We found that the broadening of the peak is dominated by diffusion for small t. Figure 5 shows that this universal behavior breaks down after a certain time and W goes to or through a maximum value. In this section we will explain two aspects of this late-stage behavior with the analogy of a Brownian particle in a potential well, discussed in Sec. II B.

First, we want to discuss the maximum of W. The maximum can have two different origins, illustrated by Fig. 5. For small values of Pe, the variation in the viscous potential V (6) between $z=0$ and $z=L$ is small. Ions tend to distribute uniformly by diffusion [see Fig. 5(a)]. It follows from the definition of W (15) that in this case $W \to L/2$ (and $W/\xi = \mathrm{Pe}/2$). The situation is different when Pe is high [see Fig. 5(b)]. The spatial variation in V influences the ion distribution. The ions are trapped in a region close to $z=0$, where V reaches its minimal value. As a consequence, $W \ll L/2$. In Fig. 4(a), it can be seen that for Pe$=0.1$ and 0.2 the peak width W is purely limited by the sample size, because $W/\xi = \mathrm{Pe}/2$ at the maximum. For Pe$=2$, 4 and 10 the peak width saturates far below $L/2$, indicating that the shape of the viscous potential limits the width of the density peak. This is

confirmed by the fact that for Pe=4 and 10 the peak width even goes through a maximum. The depth of the viscous potential increases over time [see Eq. (6)], because θ decreases during the drying process, driving the sharpening of the density peak.

Second, we want address the point where W starts to deviate from $\sqrt{t}$ for Pe$\geqslant$1. It follows from Sec. III C that these deviations are due to convection. It is interesting to see that the point where this occurs seems to be independent of Pe ($W/\xi \approx 0.2$, $\sqrt{Dt}/\xi \approx 0.27$). To understand this phenomenon we have to consider the viscous-potential difference ΔV experienced by an ion when it moves from $z=0$ to $z=W$. When we assume that $\theta \approx \varepsilon$, it follows from (6) that

$$\Delta V = \frac{W}{\xi} - \frac{1}{2\,\mathrm{Pe}}\left(\frac{W}{\xi}\right)^2. \tag{18}$$

Given that $W/\xi \approx 0.2$, ΔV increases from $\sim$0.18 to 0.2, when Pe increases from 1 to infinity. This explains why the point where deviations set in is not very sensitive to Pe. To explain why convection becomes important at this particular magnitude of ΔV ($\sim$0.2), it suffices to point to the fact that this is the lower bound of the crossover regime.

IV. ANALYTIC SOLUTIONS

An important outcome of our numerical calculations is the universal behavior of the excess ion density $\rho^{\sigma}(z,t)$ in the beginning of the drying process. At this stage of the process $\rho^{\sigma}(z,t)$ does not depend on L. With the help of the numerical results we suggested a particular solution: Eq. (17). Here we will show that there is indeed an analytical equation for $\rho^{\sigma}(z,t)$.

First, we rewrite the convection–diffusion equation and its boundary conditions (2) by using $\rho(z,t)=\rho^{*}+\rho^{\sigma}(z,t)$ and Eqs. (4) and (5):

$$\begin{aligned}
&\frac{\partial \rho^{\sigma}}{\partial t} = D\frac{\partial}{\partial z}\left(\frac{\partial \rho^{\sigma}}{\partial z} - U\rho^{\sigma}\right),\\
&\frac{\partial \rho^{\sigma}}{\partial z} + \rho^{\sigma}\frac{h}{\theta D} + \langle\rho\rangle/\xi = 0, \quad \text{at } z=0,\\
&\frac{\partial \rho^{\sigma}}{\partial z} = 0, \quad \text{at } z=L.
\end{aligned} \tag{19}$$

The interesting difference between (2) and (19) is the source term introduced via the boundary conditions. Note that $\rho^{\sigma}(z,0)=0$. Therefore, in the beginning of the process, the terms $U\rho^{\sigma}$ and $\rho^{\sigma}h/\theta D$ are small and can be neglected, resulting in the following set of equations:

$$\begin{aligned}
&\frac{\partial \rho^{\sigma}}{\partial t} = D\frac{\partial^2 \rho^{\sigma}}{\partial z^2},\\
&\frac{\partial \rho^{\sigma}}{\partial z} + \langle\rho\rangle/\xi = 0, \quad \text{at } z=0,\\
&\frac{\partial \rho^{\sigma}}{\partial z} = 0, \quad \text{at } z=L.
\end{aligned} \tag{20}$$

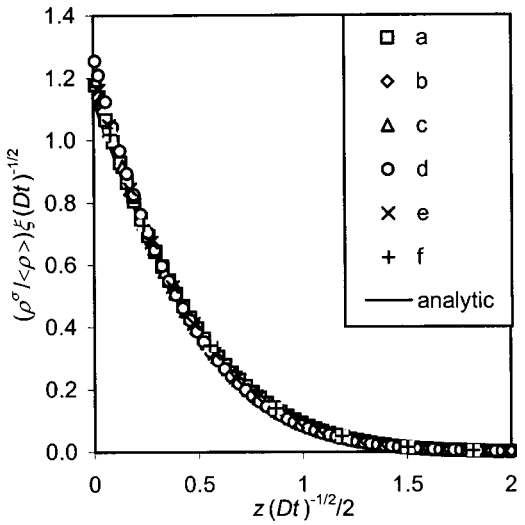

FIG. 6. Scaled density profiles for different values of Pe and $\sqrt{Dt}/\xi$: (a) (Pe, $\sqrt{Dt}/\xi$)=(1,0.15), (b) idem=(2,0.10), (c) idem=(2,0.20), (d) idem=(2,0.30), (e) idem=(4,0.20), and (f) idem=(10,0.16). The solid line represents the analytical solution, given by Eq. (22).

This set of equations can be solved via a Laplace transformation. The solution in the Laplace domain is given by

$$\tilde{\rho}^{\sigma}(z,s) = \frac{\langle\rho\rangle}{\xi}\sqrt{\frac{D}{s^3}}\frac{\cosh[(z-L)\sqrt{s/D}]}{\sinh(L\sqrt{s/D})}. \tag{21}$$

When we assume that $L\to\infty$, which is reasonable for small t, we find the following relation for $\rho^{\sigma}(z,t)$ by inverse Laplace transformation:[16]

$$\rho^{\sigma}(z,t) = \langle\rho\rangle\frac{2}{\sqrt{\pi}}\frac{\sqrt{Dt}}{\xi}\left[\exp\left(-\frac{z^2}{4Dt}\right) - \frac{z}{\sqrt{Dt}}\int_{z/2\sqrt{Dt}}^{\infty}\exp(-\lambda^2)\,d\lambda\right]. \tag{22}$$

With the help of this equation we obtain the following for H and W [Eq. (15)]:

$$W(t) = \frac{4}{3\sqrt{\pi}}\sqrt{Dt}, \tag{23}$$

$$H(t) = \frac{2}{\sqrt{\pi}}\frac{\sqrt{Dt}}{\xi}. \tag{24}$$

In Figs. 4(a) and 4(b) we have plotted (23) and (24) together with the numerical results. For small t Eqs. (23) and (24) are in excellent agreement with the numerical data.

The ultimate test for Eq. (22) is to compare it with density profiles for various sample sizes at different times. In principle, all curves should coincide when $\rho^{\sigma}\xi/\sqrt{Dt}$ is plotted as a function of $z/2\sqrt{Dt}$. In Fig. 6 we have plotted $\rho^{\sigma}\xi/\langle\rho\rangle\sqrt{Dt}$ for a variety of Pe numbers and at different times. The agreement between the analytical equation (22) and the FD results is very good. Small deviations are visible around $z=0$. These deviations systematically grow with $\sqrt{Dt}/\xi$, which is logical for a short-term solution [Eq. (22)].

The fact that Eq. (22) is in good agreement with the numerical calculations confirms the idea that we already put forward in our discussion in Sec. III C, namely that the density peak initially broadens purely by diffusion. We explicitly assumed this when we went from Eq. (19) to (20).

We can conclude that we have an analytical equation for the shape of the density profile in the beginning of the drying process. According to Figs. 4 and 6, the analytical expression holds for $\sqrt{Dt}/\xi < 0.27$ ($\mathrm{Pe} \geqslant 1$). By using (24), it can be shown that the maximum excess density reached before $\sqrt{Dt}/\xi = 0.27$ is ~30% of the average density. This means that we should be able to study this short-term behavior with NMR.[3]

V. CONCLUSIONS

A. Ion distribution

We developed a simple model based on the convection–diffusion equation for the transport behavior of ions in a drying porous medium. The input parameters of the model are the drying rate h, porosity ε, diffusion constant D, and sample size L. We showed that ions behave like Brownian particles trapped in a potential well of viscous origin. The ''viscous'' potential has a minimum at the evaporating surface. We have found that the depth of the viscous potential is proportional to $\mathrm{Pe} \equiv hL/\varepsilon D$ (i.e., the Peclet number at $t=0$ at the evaporating surface; a measure for the importance of convection compared to diffusion). Due to this potential minimum ions are ''attracted'' by and accumulate at the evaporating surface. Therefore, the driving force for accumulation is convection.

We made numerical calculations to study the behavior of the density profiles as a function of time for different values of Pe. When $\mathrm{Pe} \ll 1$ the ions remain uniformly distributed throughout the system. Strong accumulation at the evaporating surface occurs for $\mathrm{Pe} \gg 1$. Crossover behavior is found for $\mathrm{Pe} \approx 1$.

Initially, at the evaporating surface, a sharp peak in the density profile develops as a result of the convection of ions. This peak broadens by diffusion. In the beginning this broadening process is solely determined by diffusion and independent of Pe. In a later stage of the process, the width of the density peak saturates either by the finite size of the sample or by the fact that ions experience a significant change in the viscous potential.

An analytic expression can be obtained for the short-term behavior of the density peak, which is in perfect agreement with numerical calculations.

In the near future we hope to be able to compare the outcomes of the model with NMR experiments. We can conclude from our model that these experiments should be done for different values of Pe, especially around $\mathrm{Pe} = 1$. The easiest way to do this in practice is by varying the sample size L and the drying rate h.

B. Implications for crystallization

Although we have not incorporated crystallization in our model, the results indicate where the first crystals will be formed. Crystallization will take place when the salt content of the liquid phase reaches the saturation concentration. When $\mathrm{Pe} \ll 1$, the peak in the density profile is negligible and it is likely that the first crystals will be formed both in the bulk and at the interfaces of the material. For high values of Pe the density peak at the evaporating surface will reach the saturation concentration long before it is reached in the bulk of the material. As a consequence, the salt starts to crystallize at the interfaces and not in the bulk of the material. The size of the region where these first salt crystals are located will be of the order ξ.

We can conclude that given a particular porous material and salt concentration, salt crystallization at surfaces will be promoted by both a higher drying rate and a larger system size, and that these effects can be explained with our model.

ACKNOWLEDGMENT

This project was financially supported by the Dutch Technology Foundation (STW).

[1] S. Z. Lewin, ''The mechanism of masonry decay through crystallisation,'' in *Conservation of Historic Stone Buildings and Monuments* (National Acad. Press, Washington, DC, 1980), p. 180.
[2] I. S. Evans, ''Salt crystallization and rock weathering: a review,'' Rev. Geomor. Dyn. **19**, 155 (1970).
[3] L. Pel, K. Kopinga, and E. F. Kaasschieter, ''Saline absorption in calcium-silicate brick observed by NMR scanning,'' J. Phys. D **33**, 1380 (2000).
[4] L. Pel, H. Brocken, and K. Kopinga, ''Determination of moisture diffusivity in porous media using moisture concentration profiles,'' Int. J. Heat Mass Transf. **39**, 1273 (1996).
[5] J. van Brakel, ''Mass transfer in convective drying,'' Adv. Drying **1**, 217 (1980).
[6] Y. T. Puyate, C. J. Lawrence, N. R. Buenfeld, and I. M. McLoughlin, ''Chloride transport models for wick action in concrete at large Peclet number,'' Phys. Fluids **10**, 566 (1998).
[7] Y. T. Puyate and C. J. Lawrence, ''Wick action at moderate Péclet number,'' Phys. Fluids **10**, 2114 (1998).
[8] L. Pel, A. A. J. Ketelaars, O. C. G. Adan, and A. A. van Well, ''Determination of moisture diffusivity in porous media using scanning neutron radiography,'' Int. J. Heat Mass Transf. **36**, 1261 (1993).
[9] J. Bear and Y. Bachmat, *Introduction to Modelling of Transport Phenomena in Porous Media* (Kluwer, Dordrecht, 1990).
[10] A. Katchalsky and P. F. Curran, *Nonequilibrium Thermodynamics in Biophysics* (Harvard University Press, Cambridge, 1965), p. 133.
[11] P. Wong,''Conductivity, permeability and electrokinetics,'' in *Methods in the Physics of Porous Media*, edited by P. Wong (Academic, London, 1999).
[12] F. A. L. Dullien, *Porous Media* (Academic, New York, 1979), pp. 343–347.
[13] D. Stauffer and A. Aharony, *Introduction to Percolation Theory*, 2nd ed. (Taylor & Francis, London, 1991), p. 17.
[14] H. Risken, *The Fokker–Planck Equation* (Springer-Verlag, Berlin, 1989), pp. 4–9.
[15] Y. Le Bray and M. Prat, ''Three-dimensional pore network simulation of drying in capillary porous media,'' Int. J. Heat Mass Transf. **42**, 4207 (1999).
[16] F. Oberhettinger and L. Badii, *Tables of Laplace Transforms* (Springer-Verlag, Berlin, 1973), p. 258.